Science Advances
AAAS

advances.sciencemag.org/cgi/content/full/6/51/eabc8900/DC1

Supplementary Materials for

Organic monolayers disrupt plastic flow in metals

Tatsuya Sugihara, Anirudh Udupa, Koushik Viswanathan, Jason M. Davis, Srinivasan Chandrasekar*

*Corresponding author. Email: chandy@purdue.edu

Published 16 December 2020, *Sci. Adv.* **6**, eabc8900 (2020)
DOI: 10.1126/sciadv.abc8900

The PDF file includes:

Sections S1 to S3
Figs. S1 and S2
References

Other Supplementary Material for this manuscript includes the following:

(available at advances.sciencemag.org/cgi/content/full/6/51/eabc8900/DC1)

Movie S1

Supplementary Information

S1 Evaluation of Cut Surface

The quality of the (residual) cut surface of the workpiece, viz, the surface in the wake of the wedge, after approximately 6 s of cutting, was measured using a laser scanning confocal microscope (Keyence VK-X250). **Fig. S1(A)** clearly shows that the arithmetic average surface roughness (R_a) of the cut surface sharply decreases when the SAM chain length exceeds 8. Thus the change in flow mode, from sinuous to segmented caused by the MC effect, also leads to significant improvement in cut surface quality. In cutting of the bare Al, CH_3(3) and CH_3(6) workpieces, where sinuous flow is dominant and there is no MC effect, the R_a is quite large, $\sim$12.5 μm, see **Fig. S1(A)**; and the surface is pockmarked by periodic cracks and tears due to material pull-out (**Fig. S1(B)**). The rough surfaces, with material pullout, are a consequence of the large forces associated with the sinuous flow; and the periodic pull-out is the cause of the oscillations seen in the force trace (see **Fig. 2A** of main text). This type of rough surface was seen to occur consistently with the sinuous flow. In contrast, the surfaces produced with the long-chain SAMs (CH_3(10), CH_3(16), and SA(17)), wherein segmented flow is observed, were always smooth ($R_a = 0.5$ μm), see **Fig. S1(A)** and **Fig. S1(C)**, indicating that the MC effect should be beneficial also for enhancing quality of machined products.

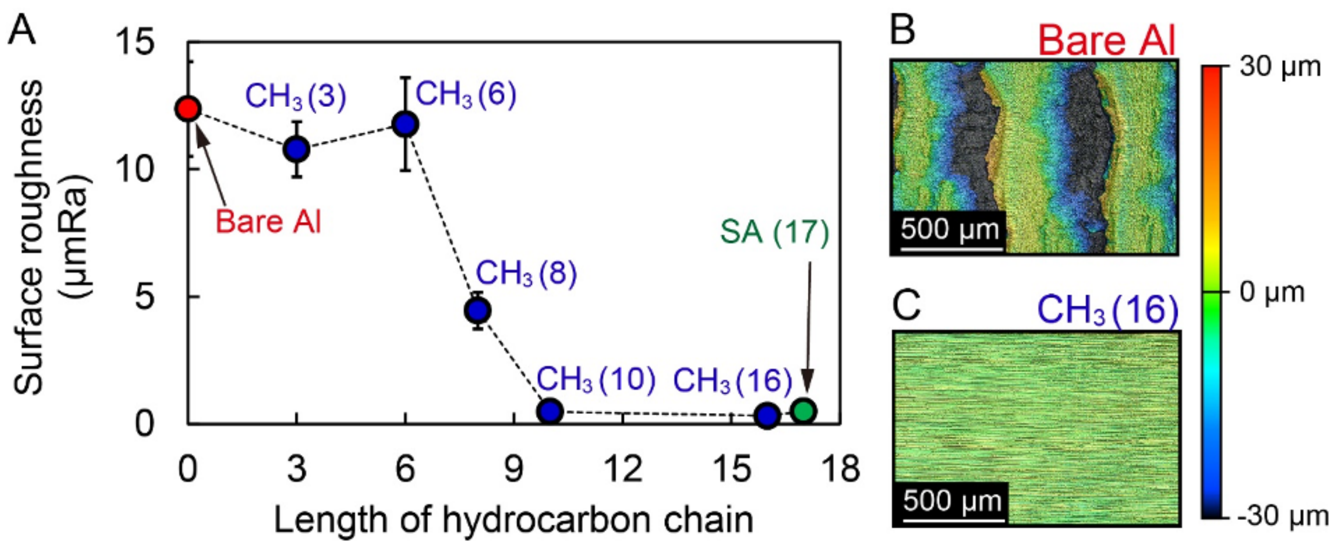

Figure S1: Characterizing cut surface quality with and without the MC effect. A) Variation of arithmetic average surface roughness (R_a) with SAM chain length. There is more than an order of magnitude improvement in the surface roughness (R_a) for chain lengths ≥ 10 (MC effect), compared to chain lengths < 8 and the bare Al case (no MC effect); this improvement is concomitant with the large force reduction due to the MC effect (**Fig. 2B**). B) Cut surface of bare Al showing extremely poor surface quality with periodic cracks and tears. C) Cut surface of workpiece produced with $CH_3$16 SAM layer showing excellent surface quality, with surface devoid of cracks and tears.

S2 Continuum Model

In order to study ductile versus brittle behavior of crystals, a key feature of sinuous-to-segmented flow transition underlying the MC effect, we use the framework developed by Rice and Thomson [38].Their approach is to explore the behavior of an atomically-sharp notch tip in a material that is loaded remotely. When the load reaches a value equal to the Griffith stress, depending on the material properties, the notch will do one of the following two things, 1) allow a crack to propagate into the material, thus extending the length of the crack (brittle) or 2) emit dislocations and get blunted in the process (ductile). Crystals for which dislocation emission is spontaneous can be expected to be ductile and others wherein there exists a large energy barrier for this emission can be expected to be good candidates for brittle cleavage. Using such an approach they were able to predict the ductility or lack thereof of several metallic and ionic crystals. We extend this framework to probe how the behavior of a crystal changes in the presence of a surface-stress at the notch-tip induced by an adsorbate.

In order to assess, the effect of the surface-stress using the Rice-Thomson model, consider a

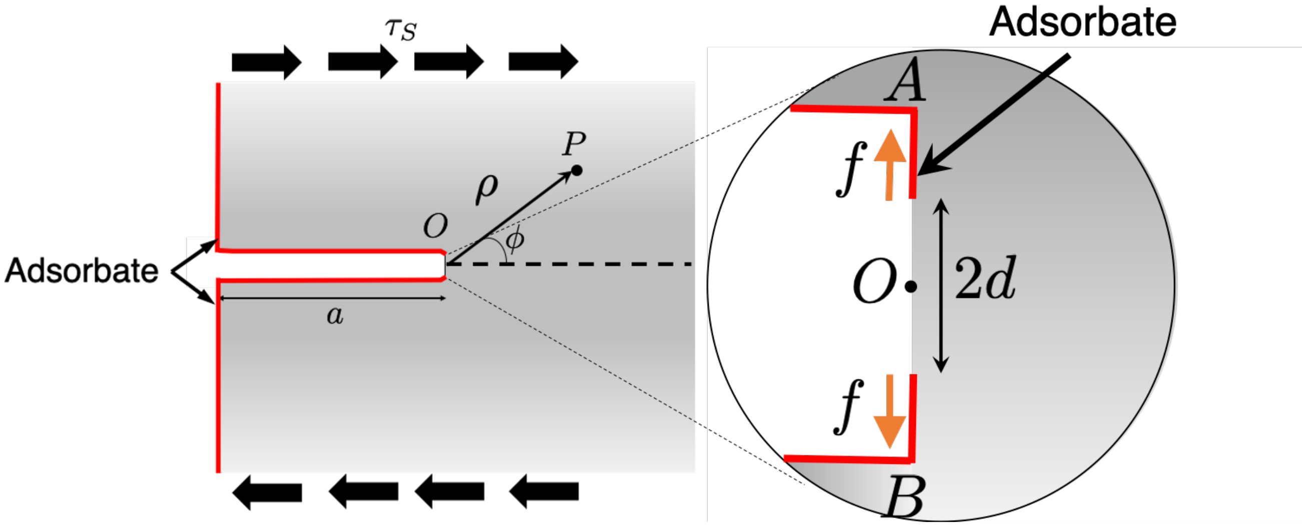

Figure S2: Schematic of an elastic half-space with a notch of length a at the origin. The body is assumed to be loaded remotely with a shear stress, τ_S. The free surface of the body is assumed to be covered by an adsorbate. The adsorbate induces a change in the surface stress, f. The coverage is assumed complete except at the tip of the notch, O. At O there exists a small region of length $2d$ where there is no adsorbate. This non-homogenous coverage induces a force dipole, $M = 2fd$. The problem is formulated to calculate the stress in the vicinity of the notch due to the combined remote loading and the force dipole. This stress is then used to evaluate the propensity of the notch to emit a dislocation.

semi-infinite elastic body with a notch at the surface, shown schematically in **Fig. S2**. Let the length of the notch be a. Assume further that the free-surface of the body, including the two notch faces are covered by an adsorbate. The adsorbate, where it is present, induces a change in the surface-stress, f. Let the coverage of the adsorbate be perfect except at the tip of the notch, O, where there is a very small region of length $2d$ that is not covered by the adsorbate.

We wish to evaluate the change in the bulk stress field due to the modified surface stress. A surface-stress can influence the bulk stress field either from regions where it is not homogeneous or from regions having curvature [42]. The role of curvature is only to influence the hydrostatic component of the stress and hence has no influence the movement of dislocations. Thus ignoring curvature effects the only regions from which the surface-stress can “load” the crystal are near the point of surface-stress discontinuity, i.e. vicinity of point O. Since there is a discontinuous change in the surface-stress where the adsorbate coverage ends, the “loading” from the surface-stress field can be replaced by two line loads of magnitude f acting in opposite directions at a distance $2d$ apart around the point O, as shown in **Fig. S2(right)**. Since this loading consists of two forces of equal magnitude acting in opposite directions and situated a small distance apart, we denote it as a force-dipole loading system.

S2.1 Elastic stress field due to force-dipole

The elastic-stress field due to the force-dipole can be estimated using the Flamant solution. This solution for a single line load parallel to the half-space is,

$$\sigma_{\rho\rho} = -\frac{2f}{\pi\rho}\cos(\theta) \tag{1}$$

$$\sigma_{\theta\theta} = 0 \tag{2}$$

$$\tau_{\rho\theta} = 0 \tag{3}$$

where θ is measured with respect to the plane boundary.

Using the superposition principle and with a suitable change of coordinates, the shear stress field due to a force-dipole acting on an elastic half-space $\tau_{\rho\phi}$, for $\rho \gg d$, is,

$$\tau_{\rho\phi} = -\frac{2fd}{\pi\rho^2}\sin(2\phi) = -\frac{M}{\pi\rho^2}\sin(2\phi) \tag{4}$$

This $\tau_{\rho\phi}$ will now be used to evaluate the force on a virtual dislocation close to the notch-tip.

S2.2 Force on a virtual dislocation

We are now in a position to evaluate the force on a virtual dislocation close to the notch-tip that is covered by an adsorbate. The Rice-Thomson model evaluates the force on the dislocation when the stress intensity factor due to the remote stress is equal to the critical stress intensity factor. The critical stress intensity factor for Mode-II loading is equal to $K_{II}^C = \sqrt{\frac{2E\gamma}{1-\nu^2}}$. A virtual dislocation close to the notch-tip experiences two forces, a Peach-Koehler force due to the shear-stress field and an image force which tends to attract it to the notch-tip. The Peach-Koehler force has two parts, one due to the remote loading and one due to the force-dipole (see Eq. 4).For a straight edge dislocation, this force equilibrium leads to

$$\underbrace{\sqrt{\frac{E\gamma b}{4\pi(1-\nu^2)\xi}}F(\phi)}_{\text{Remote loading}} \quad \underbrace{-\frac{2M}{\pi b^2\xi^2}G(\phi)}_{\text{Force dipole}} \quad \underbrace{-\frac{Eb}{8\pi(1-\nu^2)\xi}}_{\text{Image force}} = 0 \tag{5}$$

, where E is the Young's modulus, $\xi = \rho/b$ and F and G are purely functions of ϕ defined by

$$F(\phi) = \frac{3}{2}\cos(3\phi/2) + \frac{1}{2}\cos(\phi/2) \qquad G(\phi) = \sin\phi\cos\phi \tag{6}$$

Eq. 5 can then be simplified as follows,

$$\sqrt{\frac{8\pi\zeta}{\xi}}\,F(\phi) - \frac{8\eta}{\xi^2}\,G(\phi) = \frac{1}{\xi} \tag{7}$$

, where $\zeta = \gamma(1-\nu)/\mu b$ and $\eta = M(1-\nu)/\mu b^2$.

Let ξ^* denote that ξ which is a solution for Eq. 7 and hence the location where the forces on the dislocation are balanced. If $\xi^* > \xi_c$,(ξ_c is the non-dimensionalized core radius and is equal to 2 for fcc solids) then any dislocation emitted at O(**Fig. S2**) must overcome an energy barrier to leave the notch-tip. In this case, crack-propagation is the preferred mode resulting in segmented type flow. Similarly if $\xi^* < \xi_c$ then dislocations are spontaneously emitted thereby preventing crack propagation. Under this condition sinuous flow should develop. The solution to Eq. 7 is shown in **Fig. 4B** of the main text and used to discriminate between the conditions for sinuous (no MC effect, ductile) and segmented flow (MC effect, brittle).

S3 Molecular Dynamics (MD) Simulations

In order to verify the predictions of the continuum model that a modified surface-stress can indeed induce embrittlement in any otherwise ductile metal we performed simulations using the open-source software LAMMPS [43]. The model material was aluminum, simulated using the Embedded Atom Method (EAM) interatomic potential. The simulations mimic the configuration of the Rice-Thomson framework as shown in **Fig. S2**. An orthorhombic aluminum crystal ($L_x \times L_y \times L_z =$

40 nm $\times$ 5 nm $\times$ 40 nm) containing a notch is subjected to remote tensile loading. The notch was $\sim$ 2 nm in length and $\sim$ 0.8 nm in width and lies parallel to the X-direction ($\langle 100 \rangle$). Periodic boundary conditions (PBC) are imposed in the Y-direction to simulate plane-strain conditions. An NVT ensemble, with $T = 300K$, was simulated using a Langevin thermostat and a velocity-Verlet algorithm with integration time steps of 1 fs. The remote tensile loading was simulated by moving the top-row of atoms in the Z-direction, maintaining a strain-rate of $10^6\ s^{-1}$, while holding the bottom row of atoms fixed stationary.

Simulations corresponding to **Fig. 4C** (bottom row) had adsorbate atoms at the notch-tip. The adsorbate atoms were modeled as Lennard-Jones solid. This minimizes the parameters that the adsorbate brings to the simulation, such as charge of atoms, polarity etc., thereby making the results easy to interpret. The adsorbate induced surface-stress at the notch-tip was controlled by changing the equilibrium distance between the LJ adsorbate molecules. The lattice-mismatch between the LJ atoms and the aluminum atoms can be modified to control the magnitude and sign of the surface stress. In the actual experiments, the SAM molecules induce surface stress on the metal workpiece because of van-der Waals interactions between the long chain molecules, not because of a lattice mismatch.

The adsorbate induced surface stress was estimated in a separate simulation where interaction of the LJ adsorbate atoms were studied on a ($L_x \times L_y \times L_z = 75$ nm $\times$ 75 nm $\times$ 80 nm) orthorhombic aluminum crystal. Periodic boundary conditions were imposed in the X and Y directions while adsorption was allowed to occur on the planes perpendicular to the Z-axis. The surface stress is calculated using the magnitude of the interatomic forces of the surface Al atoms relative to the bulk Al atoms, utilizing the *stress/atom* routine in LAMMPS.

REFERENCES AND NOTES

1. D. Tabor, Babylonian lecanomancy: An ancient text on the spreading of oil on water. *J. Colloid Interface Sci.* **75**, 240–245 (1980).

2. J. E. Greene, Organic thin films: From monolayers on liquids to multilayers on solids. *Phys. Today* **67**, 43–48 (2014).

3. H. Rackham, *Pliny: Natural History* (Harvard Univ. Press, 1938), vol. 1, p. 361.

4. C. Tanford, *Ben Franklin Stilled the Waves* (Oxford Univ. Press, 2004).

5. P. Behroozi, K. Cordray, W. Griffin, F. Behroozi, The calming effect of oil on water. *Am. J. Phys.* **75**, 407–414 (2007).

6. A. R. C. Westwood, Tewksbury lecture: Control and application of environment-sensitive fracture processes. *J. Mater. Sci.* **9**, 1871–1895 (1974).

7. R. M. Latanision, Surface effects in crystal plasticity: General overview, *Surface Effects in Crystal Plasticity*, R. M. Latanision, J. T. Fourie, Eds. (Nordhoff, 1977), pp. 3–48.

8. S. Lynch, Hydrogen embrittlement phenomena and mechanisms. *Corrosion Rev.* **30**, 105–123 (2012).

9. J. Luo, H. Cheng, K. M. Asl, C. J. Kiely, M. P. Harmer, The role of a bilayer interfacial phase on liquid metal embrittlement. *Science* **333**, 1730–1733 (2011).

10. W. Rostoker, J. McCaughey, H. Markus, *Embrittlement by Liquid Metals* (Reinhold Pub. Corp., 1960).

11. D. H. Bangham, The Gibbs adsorption equation and adsorption on solids. *Trans. Faraday Soc.* **33**, 805–811 (1937).

12. G. Y. Gor, N. Bernstein, Revisiting Bangham's law of adsorption-induced deformation: Changes of surface energy and surface stress. *Phys. Chem. Chem. Phys.* **18**, 9788–9798 (2016).

13. R. Roscoe, Strength of metal single crystals. *Nature* **133**, 912 (1934).

14. P. Rehbinder, New physico-chemical phenomena in the deformation and mechanical treatment of solids. *Nature* **159**, 866–867 (1947).

15. R. M. Latanision, R. H. Jones, *Chemistry and Physics of Fracture* (Springer, 1987).

16. A. R. C. Westwood, J. J. Mills, Survey lecture: Applications of chemomechanical effects to fracture-dependent industrial processes, *Surface Effects in Crystal Plasticity*, R. M. Latanision, J. T. Fourie, Eds. (Nordhoff, 1977).

17. R. A. Oriani, On the possible role of the surface stress in environmentally induced embrittlement and pitting. *Scr. Metall.* **18**, 265–268 (1984).

18. P. A. Rehbinder, E. D. Shchukin, Surface phenomena in solids during deformation and fracture processes. *Prog. Surf. Sci.* **3**, 97–104 (1972).

19. J. R. Rice, J.-S. Wang, Embrittlement of interfaces by solute segregation. *Mater. Sci. Eng. A* **107**, 23–40 (1989).

20. H.-P. Chen, R. K. Kalia, E. Kaxiras, G. Lu, A. Nakano, K.-i. Nomura, A. C. T. van Duin, P. Vashishta, Z. Yuan, Embrittlement of metal by solute segregation-induced amorphization. *Phys. Rev. Lett.* **104**, 155502 (2010).

21. F. Rosei, M. Schunack, Y. Naitoh, P. Jiang, A. Gourdon, E. Laegsgaard, I. Stensgaard, C. Joachim, F. Besenbacher, Properties of large organic molecules on metal surfaces. *Prog. Surf. Sci.* **71**, 95–146 (2003).

22. H. Yeung, K. Viswanathan, W. D. Compton, S. Chandrasekar, Sinuous flow in metals. *Proc. Natl. Acad. Sci. U.S.A.* **112**, 9828–9832 (2015).

23. A. Udupa, K. Viswanathan, M. Saei, J. B. Mann, S. Chandrasekar, Material-independent mechanochemical effect in the deformation of highly strain-hardening metals. *Phys. Rev. App.* **10**, 014009 (2018).

24. A. Udupa, K. Viswanathan, J. M. Davis, M. Saei, J. B. Mann, S. Chandrasekar, A mechanochemical route to cutting highly strain-hardening metals. *Tribol. Lett.* **67**, 4 (2019).

25. N. Beckmann, P. A. Romero, D. Linsler, M. Dienwiebel, U. Stolz, M. Moseler, P. Gumbsch, Origins of folding instabilities on polycrystalline metal surfaces. *Phys. Rev. Appl.* **2**, 064004 (2014).

26. A. Ulman, Formation and structure of self-assembled monolayers. *Chem. Rev.* **96**, 1533–1554 (1996).

27. R. Berger, E. Delamarche, H. P. Lang, C. Gerber, J. K. Gimzewski, E. Meyer, H.-J. Güntherodt, Surface stress in the self-assembly of alkanethiols on gold. *Science* **276**, 2021–2024 (1997).

28. G. Wu, H. Ji, K. Hansen, T. Thundat, R. Datar, R. Cote, M. F. Hagan, A. K. Chakraborty, A. Majumdar, Origin of nanomechanical cantilever motion generated from biomolecular interactions. *Proc. Natl. Acad. Sci. U.S.A.* **98**, 1560–1564 (2001).

29. A. W. Adamson, *Physical Chemistry of Surfaces* (John Wiley & Sons, 1990).

30. D. L. Allara, R. G. Nuzzo, Spontaneously organized molecular assemblies. 1. Formation, dynamics, and physical properties of n-alkanoic acids adsorbed from solution on an oxidized aluminum surface. *Langmuir* **1**, 45–52 (1985).

31. Y.-J. Kim, K.-H. Lee, H. Sano, J. Han, T. Ichii, K. Murase, H. Sugimura, Surface chemical conversion of organosilane self-assembled monolayers with active oxygen species generated by vacuum ultraviolet irradiation of atmospheric oxygen molecules. *Jpn. J. Appl. Phys.* **47**, 307–312 (2008).

32. A. Ulman, *An Introduction to Ultrathin Organic Films: From Langmuir-Blodgett to Self-Assembly* (Academic Press, 2013).

33. C. D. Bain, E. B. Troughton, Y. T. Tao, J. Evall, G. M. Whitesides, R. G. Nuzzo, Formation of monolayer films by the spontaneous assembly of organic thiols from solution onto gold. *J. Am. Chem. Soc.* **111**, 321–335 (1989).

34. D. K. Owens, R. C. Wendt, Estimation of the surface free energy of polymers. *J. Appl. Polym. Sci.* **13**, 1741–1747 (1969).

35. The specific cutting force for hard steel is ~4050 MPa, translating to a force of 364 N for h_0 of 50 μm and width of 3 mm used in our experiments. See link for more information: http://www.mitsubishicarbide.net/contents/mhg/enuk/html/product/technical.

36. M. C. Shaw, *Metal Cutting Principles* (MIT Press, 1957).

37. J. Fritz, Cantilever biosensors. *Analyst* **133**, 855–863 (2008).

38. J. R. Rice, R. Thomson, Ductile versus brittle behaviour of crystals. *Philos. Mag.* **29**, 73–97 (1974).

39. F. Spaepen, Interfaces and stresses in thin films. *Acta Mater.* **48**, 31–42 (2000).

40. N. Badwe, X. Chen, D. K. Schreiber, M. J. Olszta, N. R. Overman, E. K. Karasz, A. Y. Tse, S. M. Bruemmer, K. Sieradzki, Decoupling the role of stress and corrosion in the intergranular cracking of noble-metal alloys. *Nat. Mater.* **17**, 887–893 (2018).

41. H.-J. Jin, J. Weissmüller, A material with electrically tunable strength and flow stress. *Science* **332**, 1179–1182 (2011).

42. R. Thomson, T.-J. Chuang, I.-H. Lin, The role of surface stress in fracture. *Acta Metall.* **34**, 1133–1143 (1986).

43. S. Plimpton, Fast parallel algorithms for short-range molecular dynamics. *J. Comput. Phys.* **117**, 1–19 (1995).